buildings

Article

Study on Cyclic Shear Properties of Siliceous Sand–Steel Interface under Different Normal Loading Conditions

Yongming Ma [1], Jukun Guo [2,3,*], Rui Wang [4], Qingyao Zhang [5], Qingxin Zhang [5], Jin Li [1] and Shen Zuo [1]

1 Civil Engineering Institute of Transportation, Shandong Jiaotong University, Jinan 250357, China; mym_sdjtu@126.com (Y.M.)
2 Department of Highway and Architecture, Shandong Transport Vocational College, Weifang 261206, China
3 Highway College, Chang'an University, Xi'an 710064, China
4 School of Civil and Hydraulic Engineering, Ningxia University, Yinchuan 750014, China; wryj_1996@163.com
5 School of Civil Engineering and Architecture, Xi'an University of Technology, Xi'an 710048, China; zhqx1122@163.com (Q.Z.); zqy18006461026@163.com (Q.Z.)
* Correspondence: gjk_1986@126.com

Abstract: It is of great significance to deeply understand the stress damage mechanism of the pile–soil interface under cyclic loading for the safety control of engineering entities. Large-scale self-developed shear equipment was used to conduct cyclic shear tests of the interface between steel and siliceous sand, and the macroscopic shear characteristics and particle crushing characteristics were analyzed. Finally, the interface micro characteristics were analyzed through numerical simulation. The results indicate that the interface peak shear stress under constant stress conditions mainly exhibits strengthening characteristics, while under constant stiffness conditions it exhibits weakening characteristics. The position of the relationship curve between shear stress and normal stress gradually moves towards the direction of low normal stress as the experiment progresses, and the distance between the curves gradually decreases. The degree of particle breakage increases with the number of cycles but is mainly concentrated in the first few cycles. The principal stress is proportional to the normal stress, and its rotation degree gradually weakens with the normal stress. The contact number of particles at any angle increases with the normal stress.

Keywords: siliceous sand; normal load; constant stress; constant stiffness; cyclic shear characteristics; numerical simulation

Citation: Ma, Y.; Guo, J.; Wang, R.; Zhang, Q.; Zhang, Q.; Li, J.; Zuo, S. Study on Cyclic Shear Properties of Siliceous Sand–Steel Interface under Different Normal Loading Conditions. *Buildings* **2023**, *13*, 2241. https://doi.org/10.3390/buildings13092241

Academic Editor: Harry Far

Received: 2 August 2023
Revised: 27 August 2023
Accepted: 1 September 2023
Published: 4 September 2023

1. Introduction

Sand is a common and representative geotechnical medium [1,2], which is widely distributed in coastal zones, rivers, and foothills due to geographical conditions such as terrain and sedimentary environment. In recent years, with the rapid development of economy, more and more energy projects and high-speed transportation projects are built along rivers and coastal areas, such as offshore wind turbines [3,4], offshore drilling platforms, sea crossing bridges, etc. These projects need to have high overturning resistance and bear large superstructure loads. Pile has become the foundation form of primary consideration in the design of these projects because of its strong bearing capacity and high degree of construction machinery [5,6]. In the field of wind power engineering, the development trend of "large-scale" and "deepwater" has brought many technical challenges. Wind turbines bear significant environmental loads such as wind and waves, which poses serious challenges to the design of offshore wind turbine foundations. As shown in Figure 1, among the three types of deep-water wind turbine foundation forms, the upper overturning moment is mainly transmitted to the lower foundation in the form of vertical loads [7]. Under cyclic loads caused by wind, waves, and blade rotation, the repeated shear between the pile and soil causes a weakening of the pile side friction, which has a significant impact on the mechanical properties of the pile–soil interface and can potentially damage the bearing capacity of the pile foundation [8].

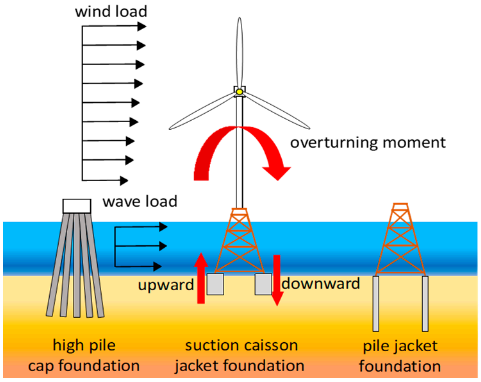

Figure 1. Types of deep-water foundation for wind turbines.

Some scholars have studied the effects of factors such as cyclic shear amplitude and sand particle type on the strength weakening of the pile soil interface through model pile loading tests [9–11] and believe that the reduction in interface strength mainly depends on the magnitude of cyclic load. They have proposed a "cyclic slip" model to simulate the strength weakening process of the pile–soil interface [12]. In addition, some scholars, combined with the indoor model pile loading test [13,14], used modified triaxial equipment to explore the evolution the law of pile side friction characteristics under cyclic loading [15]. It is found that the initial cyclic shear causes obvious particle breakage, leading to a large reduction in the normal stress and a significant weakening of the interface shear stress. In addition to model tests, different types of interface shear equipment are used to conduct structural sand interface shear tests under the influence of multiple factors. It is an important way for many scholars to explore the shear characteristics of interfaces. For example, using an interface torsion shear apparatus [16], small amplitude cyclic shear is performed after large displacement monotonic shear. The experiment simulated the interface state of the pile after being driven into the soil layer. Explore the effects of factors such as normal phase load and shear amplitude on interface shear behavior.

In addition, a direct shear test is also an important test method to explore the interaction between pile and soil interface. A constant stress interface shear test is widely used to explore the mechanical characteristics of the interface under different normal stress conditions [17–21]. However, due to the influence of shear behavior, the contact surface soil may experience shear shrinkage or expansion in practical engineering, resulting in the normal stress of the contact surface not being constant. The constant stiffness boundary condition is closer to the actual stress state of the pile–soil contact surface than the constant stress boundary condition [22,23]. Therefore, the constant stiffness interface cyclic shear test can more realistically simulate the weakening phenomenon of pile side friction resistance under cyclic load [24]. Vangla [25] and Han [26] studied the effects of factors such as particle size, particle gradation, and particle shape on the interface friction angle using a constant stiffness direct shear device. The results indicate that particle size has a significant impact on interface strength, and the interface friction angle of irregularly shaped particles is greater. Rui [27] further studied the shear state of calcareous sand under constant stiffness cyclic shear using a transparent observation window. Research has found that, compared to monotonic shear, cyclic shear produces more fine particles, which enhances the interaction between aggregate and steel. The interface strength of cyclic shear is higher than that of monotonic shear. Tohidvand [28] studied the influence of different stress paths on the shear mechanical behavior of sand under incomplete drainage conditions using a stacked ring shear equipment, and pointed out that the initial stress in the experiment is an important parameter determining the cyclic shear behavior of sand under incomplete drainage conditions. Tarhouni [29] studied the influence of shear amplitude changes on cyclic shear dynamic and deformation characteristics under different normal stress conditions and analyzed the deformation trend of soil under different conditions. It was pointed out that shear amplitude and normal stress are the main factors affecting soil deformation. In view of this, this article selects Xiamen siliceous sand as the research object. The experiment adopts two boundary conditions: constant stiffness and constant stress. Utilize a self-developed large-scale structure soil interface cyclic shear apparatus. Cyclic shear tests were conducted on the steel siliceous sand interface under different boundary conditions. The experiment aims to explore the effects of normal stress, loading method, and number of cycles on interface shear characteristics.

2. Test Preparation

2.1. Test Equipment

This device is a large-scale interface shearing instrument independently developed by the team. The detailed schematic diagram is shown in Figure 2a, and Figure 2b shows the appearance of the actual device. The equipment consists of a shear system, a normal system, and a control acquisition system. The shear system mainly consists of a shear box, shear stress sensor, shear displacement sensor, and servo motor. The shear force is provided by a 0.75 kW servo motor, with a maximum shear force of 50 kN, a maximum range of 50 kN for horizontal load sensors, and a maximum range of 50 mm for shear displacement sensors. The normal system mainly consists of a force cylinder, a normal load sensor, and a normal displacement sensor. The maximum value of the normal load sensor is 40 kN, and the maximum value of the normal displacement sensor is 30 mm.

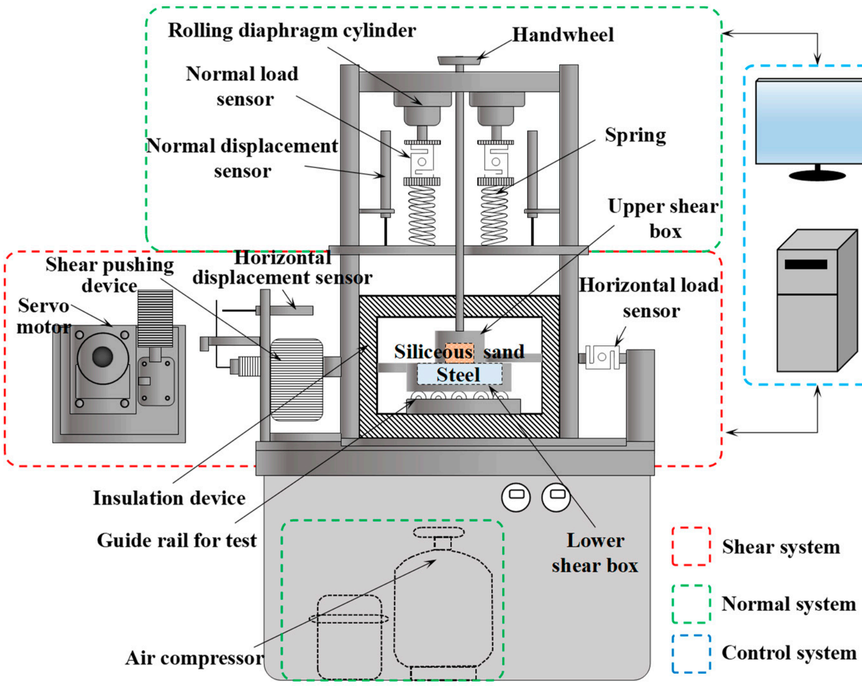

(a)

Figure 2. *Cont.*

(**b**)

Figure 2. Large interface shear equipment: (**a**) structure diagram; (**b**) equipment photo.

The test shear box is shown in Figure 3. The upper shear box is filled with soil and permeable stone, while the lower shear box is installed with structures to simulate piles in foundation engineering. There is sufficient length on both sides of the steel plate in the lower shear box. During the interface shearing process, the contact area between steel and sand remains unchanged. The experimental steel plate was mechanically processed and engraved with an inverted triangular groove on the surface, with a groove depth of 1.5 mm, a groove width of 2 mm, and a number of 20 grooves, as shown in Figure 3.

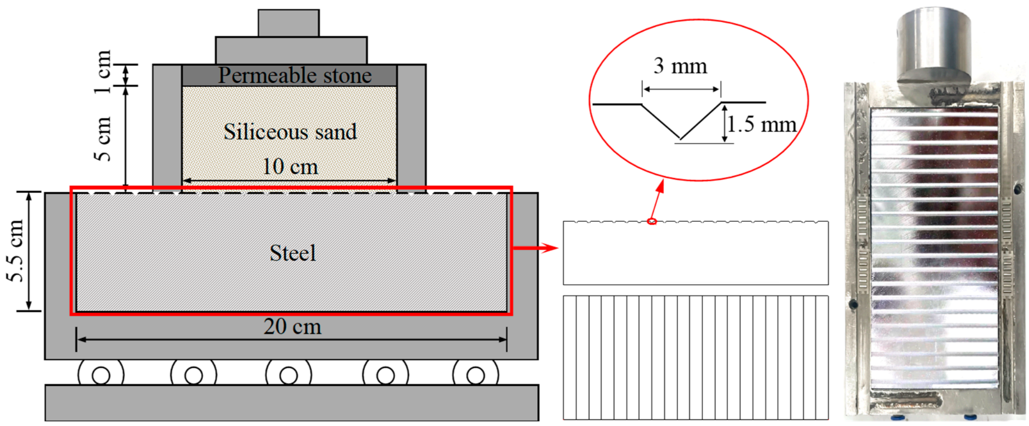

Figure 3. Test shear box.

As shown in Figure 4, the required normal stress for the test is generated by applying pressure to the cylinder. The pressure generated by the cylinder is applied to the sand in the upper shear box through a load sensor and a force transmission spring. By replacing different types of limit steel rings, the cylinder retraction under different normal stresses is restrained to achieve the goal of constant stiffness loading. The principles of constant stress and constant stiffness loading can be explained by the following equation:

$$\sigma = \sigma_0 \pm k|\delta| \quad (1)$$

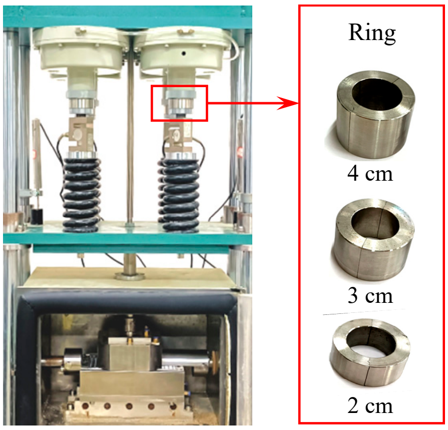

Figure 4. Constant stiffness limit device.

Among them, σ is the normal stress during the testing process, σ_0 is the initial normal stress, k is the spring coefficient (the ratio of the change in normal stress to the change in spring height), the value of k under constant stress loading is 0, the value of k under constant stiffness loading is 1.12 kN/mm, and δ is the normal displacement.

2.2. Test Soil

The sand used for the experiment is Xiamen siliceous sand. After screening, coarse sand with a particle size group of 0.5–2 mm is selected for testing. The sand particles are shown in Figure 5, with a mass ratio of 53.35% for the particle size group of 0.5–1 mm and 46.65% for the particle size group of 1–2 mm. The grading index is shown in Table 1. The main physical indicators of the sand used for the test are obtained according to the Highway Geotechnical Test Specification (JTG 3430-2020) [30], as shown in Table 2. To eliminate the influence of water content on the test results, the test sand was dried in an oven before use.

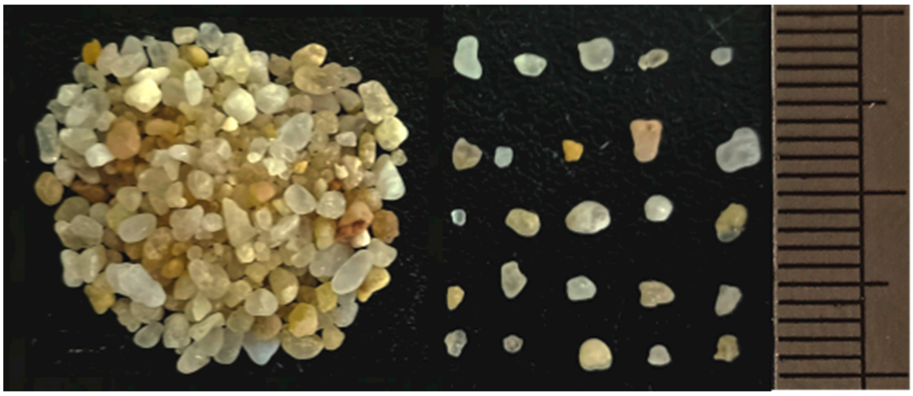

Figure 5. Siliceous sand used in the test.

Table 1. Grading index of test sand.

Characteristic Particle Size/mm				C_u	C_c
d_{10}	d_{30}	d_{50}	d_{60}		
0.57	0.74	0.96	1.10	1.94	0.87

Table 2. Main physical indicators of test Sand.

Maximum Void Ratio	Minimum Void Ratio	Test Void Ratio	Specific Gravity	Density/(g·cm^{-3})
0.671	0.520	0.535	2.65	1.73

2.3. Test Plan

The experiment adopts normal loading boundary conditions of constant stress and constant stiffness. In order to study the strength and deformation characteristics of sand under different normal stresses, the normal stress is divided into normal pressure, medium pressure, and high pressure according to the numerical value. Normal stress not exceeding 800 kPa is considered low pressure, a normal stress range from 800 to 2000 kPa is considered medium pressure, normal stress greater than 2000 kPa is considered high pressure, and normal stress applied under normal stress conditions is 200 kPa, 1100 kPa, and 2400 kPa, respectively. The maximum normal stress that the equipment can apply under constant stiffness conditions is 2000 kPa. Therefore, under constant stiffness conditions, normal stress applied is 200 kPa and 1100 kPa, respectively. The number of cycles N is 1, 5, 10, and 15, respectively, and the number of test groups is 20.

The cyclic shear displacement process is shown in Figure 6, which divides a cyclic process into four stages: ①–④. Firstly, the shear displacement increases, indicating that the experiment begins to shear forward at a shear rate of 1 mm per minute. After the shear displacement reaches 4 mm, the shear displacement begins to decrease, indicating the beginning of reverse shear until the shear displacement reaches 8 mm in this direction, and then shear to 4 mm in the positive direction, indicating the end of the entire cycle. After each group of experiments is completed, the sand in the shear box is screened to study the broken characteristics of sand particles.

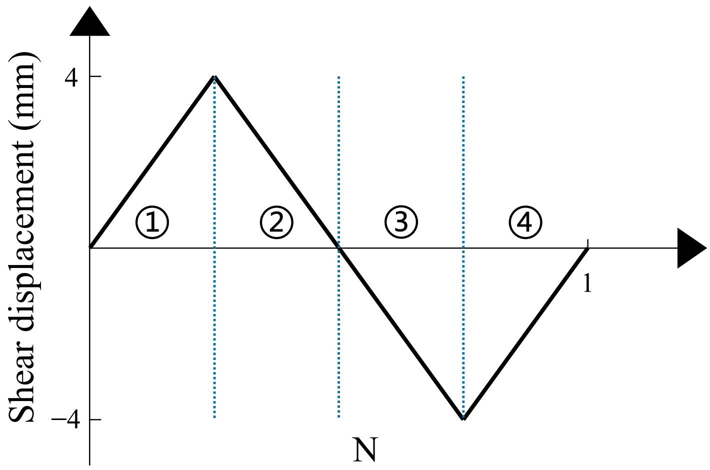

Figure 6. Schematic diagram of cyclic shear.

3. Interface Macroscopic Shear Characteristics

3.1. Change Rule of Shear Stress

The relationship between shear stress and the number of cycles of interface between steel and siliceous sand is shown in Figure 7. It can be analyzed that the shear stress exhibits a periodic variation rule with the shear time and the alternating change in shear direction. Under constant stress conditions, the peak shear stress at 200 kPa and 1100 kPa decreases first and then increases with the number of cycles. The peak shear stress at 2400 kPa increases with the number of cycles and gradually stabilizes. It can be seen that the peak shear stress at low and medium pressure shows weakening characteristics in the first few cycles of the test, while it shows certain strengthening characteristics under high pressure. Under constant stiffness conditions, the peak shear stress at 200 kPa and 1100 kPa decreases with the number of cycles, and the rate of decrease gradually slows down. The peak shear stress shows a weakening characteristic throughout the entire experiment.

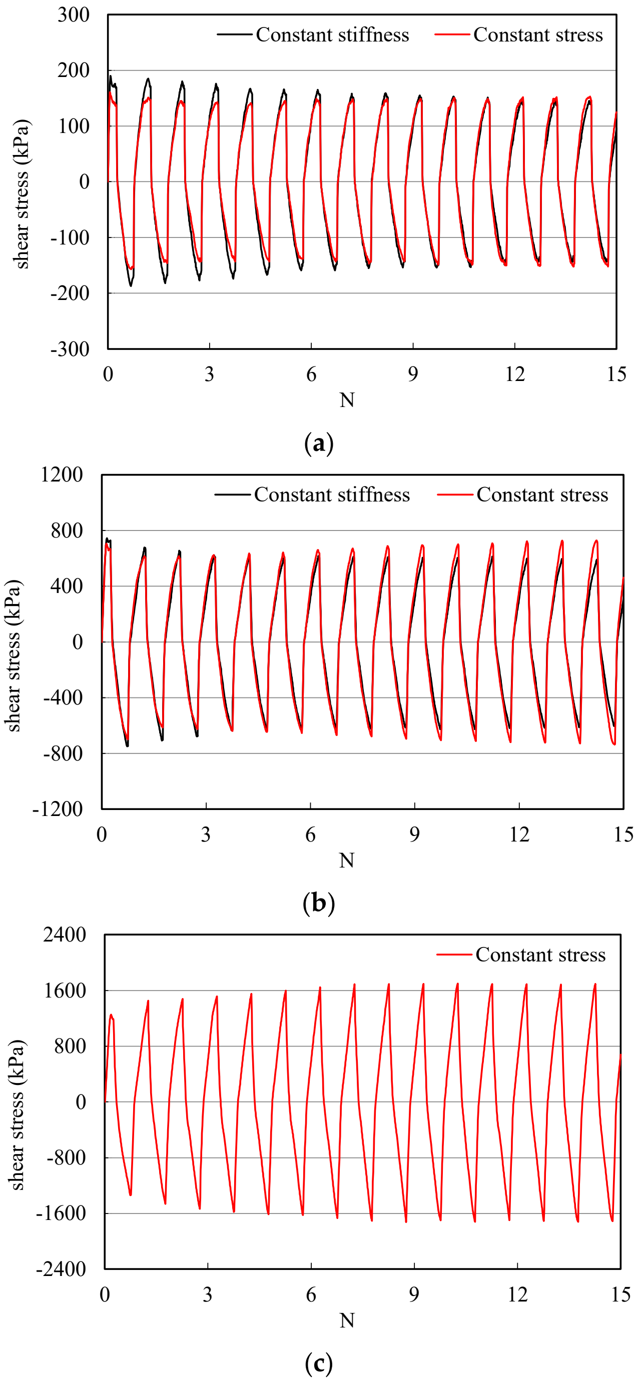

Figure 7. Variation law of interface shear stress: (**a**) cyclic shear stress curve at 200 kPa; (**b**) cyclic shear stress curve at 1100 kPa; (**c**) cyclic shear stress curve at 2400 kPa.

The relationship between shear stress and shear displacement is shown in Figure 8. It can be seen that the variation of interface shear stress with shear displacement in stage ① is consistent with the monotonic shear law of the interface. In stages ② and ③, the shear direction changes from positive to negative, and the shear stress changes from positive to negative. For a single cyclic shear, the relationship curve between shear stress and shear displacement forms a "hysteresis loop". Under constant stress conditions, the area of the "hysteresis loop" at 200 kPa and 1100 kPa shows a decreasing and then increasing trend with the number of cycles. The area of the "hysteresis loop" at 2400 kPa shows a gradually increasing trend, but the positions of the "hysteresis loop" at the 10th and 15th cycle have basically overlapped. Under constant stiffness conditions, the area of the "hysteresis loop" at 200 kPa decreases with the number of cycles. The area of the "hysteresis loop" at 1100 kPa decreases significantly from the first cycle to the fifth cycle, and the positions of the "hysteresis loop" at the fifth, tenth, and fifteenth cycles have basically overlapped.

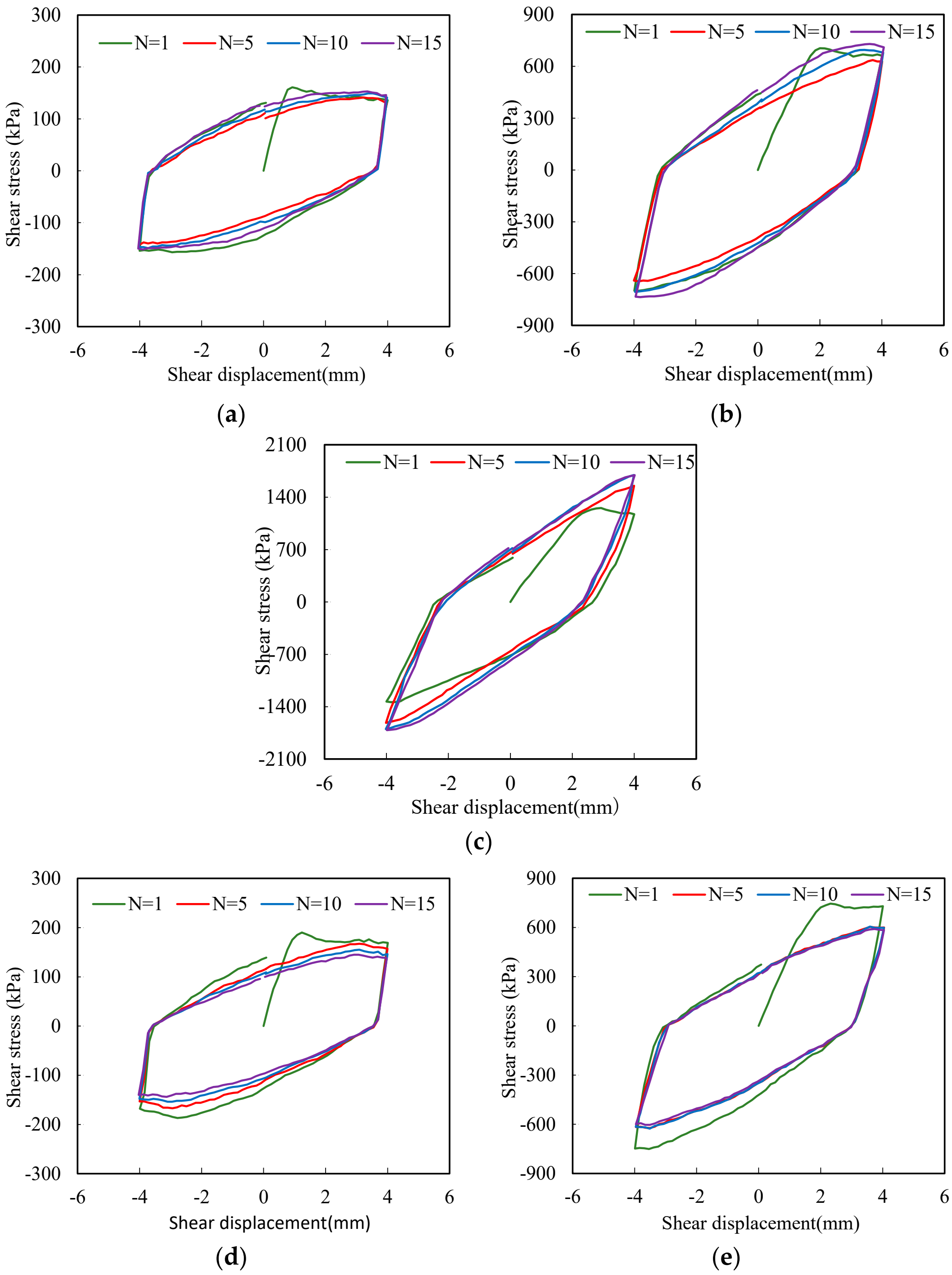

Figure 8. Relationship between shear stress and shear displacement: (**a**) constant stress normal stress 200 kPa; (**b**) constant stress normal stress 1100 kPa; (**c**) constant stress normal stress 2400 kPa; (**d**) constant stiffness normal stress 200 kPa; (**e**) constant stiffness normal stress 1100 kPa.

3.2. Change Rule of Normal Displacement

The relationship between the normal volumetric deformation characteristics of siliceous sand and the number of cyclic shear is shown in Figure 9. As the number of cyclic shear increases, siliceous sand exhibits regular deformation characteristics. An increase in normal displacement represents shear expansion and a decrease in normal displacement represents shear shrinkage. Overall, in cyclic shear experiments, the normal displacement exhibits shear shrinkage characteristics, and the degree of shrinkage is proportional to the normal stress. Under the same normal stress conditions, different loading conditions can lead to significant differences in shear deformation. It can be concluded that under the same stress conditions, the cumulative shear volume variables under constant stress loading are greater than those under constant stiffness loading. Within a single shear cycle, the volumetric characteristics exhibit regular shear shrinkage and shear expansion. The larger the normal stress, the greater the fluctuation amplitude of the relationship curve between normal displacement and the number of cycles.

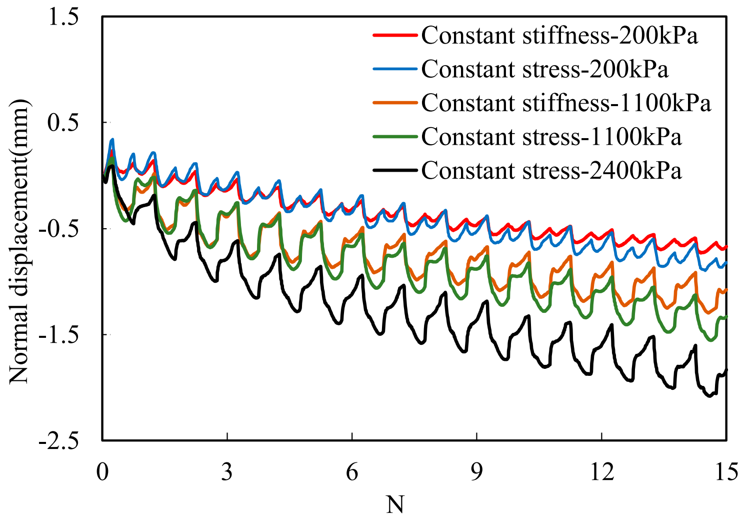

Figure 9. Relationship between normal displacement and the number of cycles.

The relationship between normal displacement and shear displacement is shown in Figure 10. It can be seen that the curve gradually moves downwards with the number of cycles, and the interval distance between the curves gradually decreases. The amplitude of the fluctuation of the curve within a single cycle gradually weakens, and the shape of the curve gradually flattens with the number of cycles. Under different experimental conditions, the variation rule of normal displacement with shear displacement varies. At 200 kPa, the volumetric characteristics of each cycle stage ① are mainly manifested as shear expansion, while the soil at stage ②, ③, and ④ exhibits volumetric characteristics of first shear shrinkage and then shear expansion. At 1100 kPa and 2400 kPa, the volumetric deformation characteristics of siliceous sand are mainly characterized by shear expansion in the stage ① of the first cycle, except for small shear shrinkage in the initial stage of the first cycle. The volumetric deformation characteristics in stages ② and ③ are similar to those at 200 kPa and are significantly weakened by normal stress at 2400 kPa; in addition, the volumetric deformation characteristics of the 5th cycle show significant shear shrinkage compared to the first cycle; the soil exhibits obvious shear expansion characteristics in stage ④, which are significantly different from the volumetric deformation characteristics at 200 kPa. Compared with the constant stress condition, the fluctuation amplitude of the normal displacement shear displacement curve under the constant stiffness condition decreases, the curve is flatter, the normal displacement of the same number of cycles is smaller, and the distance between adjacent curves is also smaller.

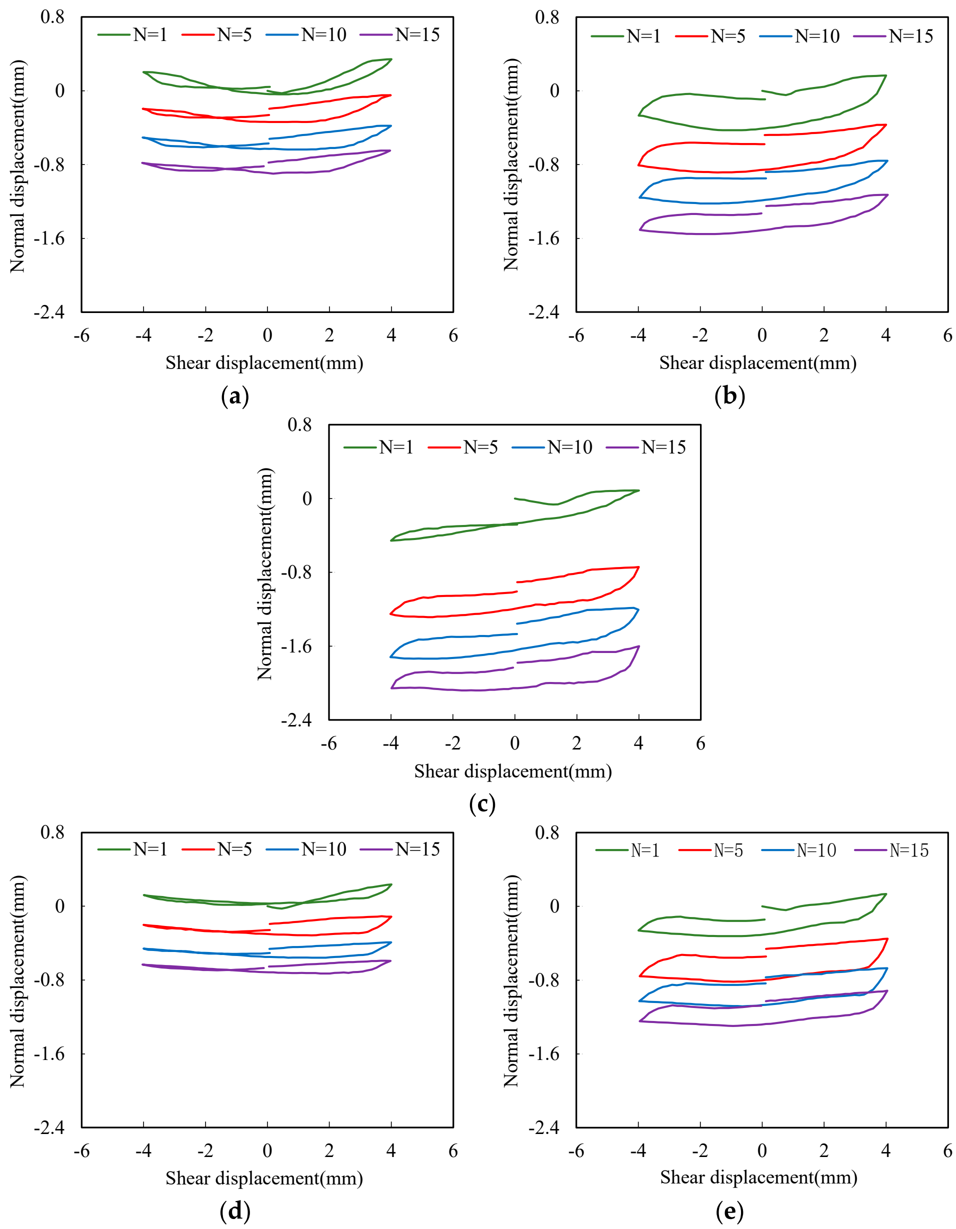

Figure 10. Relationship between normal displacement and shear displacement: (**a**) constant stress normal stress 200 kPa; (**b**) constant stress normal stress 1100 kPa; (**c**) constant stress normal stress 2400 kPa; (**d**) constant stiffness normal stress 200 kPa; (**e**) constant stiffness normal stress 1100 kPa.

3.3. Change Rule of Normal Stress

Under constant stress loading conditions, the normal stress remains unchanged in the experiment, so only the variation law of normal stress under constant stiffness loading is analyzed. The relationship between shear stress and normal stress of the interface between steel and siliceous sand under constant stiffness conditions is shown in Figure 11. It can be seen that the normal stress at 200 kPa exhibits an "increase-decrease-increase-decrease-increase" rule within a single cycle. Except for the first cycle, the decreasing amplitude of other cycles is greater than the increasing amplitude. The normal stress at 1100 kPa exhibits a "decrease-increase-decrease-increase-decrease" rule in the first cycle, and an "increase-decrease-increase" rule in the fifth, tenth, and fifteenth cycles. As the number of cycles increases, the relationship curve between shear stress and normal stress gradually moves towards the direction of low normal stress. The distance between the relationship curves of different cycles at 200 kPa gradually decreases as the number of cycles increases.

The relationship curve of the fifth cycle at 1100 kPa has a significant distance from the first cycle curve, indicating that the shear shrinkage behavior of the soil in the first five cycles is significant, and the corresponding normal stress also shows a significant decrease. Afterwards, the soil shear shrinkage significantly decreased.

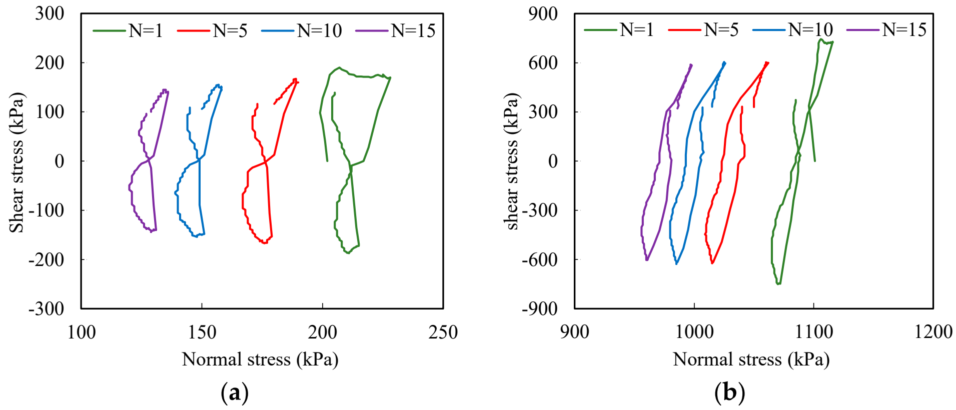

Figure 11. The relationship between shear stress and normal stress under constant stiffness conditions: (**a**) normal stress = 200 kPa; (**b**) normal stress = 1100 kPa.

4. Particle Breakage Behavior

4.1. Particle Grading Curve and Indicators

To study the variation rule of the breakage degree of siliceous sand with the number of cycles under different experimental conditions, the test sand after the end of the first, fifth, tenth, and fifteenth cycles was screened. The characteristic particle size and grading indicators are shown in Table 3. The particle grading curves of the test sand with different cycles were plotted, as shown in Figure 12. It can be seen that the characteristic particle size of siliceous sand decreases with the normal stress and number of cycles. The non-uniformity coefficient Cu and curvature coefficient Cc of sand particles are relatively close under different experimental conditions and do not show obvious changes. According to the Highway Geotechnical Test Specification (JTG 3430-2020), sand with a nonuniformity coefficient Cu > 5 and a curvature coefficient Cc that ranges from 1 to 3 is considered well graded, while other conditions are considered poorly graded. The nonuniformity coefficient Cu of siliceous sand is concentrated in the range of 1.89–1.93, and the curvature coefficient Cc is concentrated in the range of 0.87–0.88. The breakage degree of siliceous sand is relatively small, meeting the conditions for poor grading. The distance between adjacent grading curves gradually decreases with the number of cycles, indicating that particle breakage behavior mainly occurs in the first few cycles. The distance between adjacent grading curves increases with normal stress. The very small distance between adjacent grading curves at 200 kPa indicates that the breakage of siliceous sand particles mainly occurs under medium and high pressures.

Table 3. Characteristic particle size and grading indicators.

Normal Loading	σ/kPa	N	Cu	Cc	Characteristic Particle Size			
					d_{60}/mm	d_{50}/mm	d_{30}/mm	d_{10}/mm
Constant stress	200	1	1.93	0.87	1.09	0.95	0.73	0.56
		5	1.92	0.87	1.07	0.93	0.72	0.56
		10	1.91	0.87	1.06	0.92	0.71	0.55
		15	1.90	0.87	1.05	0.92	0.71	0.55
	1100	1	1.93	0.87	1.07	0.93	0.72	0.55
		5	1.93	0.87	1.04	0.91	0.70	0.54
		10	1.92	0.87	1.03	0.90	0.69	0.53
		15	1.93	0.87	1.02	0.89	0.69	0.53

Table 3. *Cont.*

Normal Loading	σ/kPa	N	Cu	Cc	Characteristic Particle Size			
					d_{60}/mm	d_{50}/mm	d_{30}/mm	d_{10}/mm
	2400	1	1.92	0.87	1.05	0.91	0.71	0.55
		5	1.92	0.88	1.01	0.89	0.69	0.53
		10	1.92	0.88	1.00	0.87	0.67	0.52
		15	1.93	0.88	0.99	0.87	0.67	0.51
Constant stiffness	200	1	1.92	0.87	1.08	0.94	0.73	0.56
		5	1.90	0.87	1.06	0.92	0.72	0.56
		10	1.89	0.87	1.05	0.92	0.71	0.55
		15	1.90	0.87	1.05	0.91	0.71	0.55
	1100	1	1.93	0.87	1.07	0.93	0.71	0.55
		5	1.93	0.87	1.04	0.91	0.70	0.54
		10	1.92	0.87	1.03	0.90	0.69	0.53
		15	1.92	0.88	1.02	0.89	0.69	0.53

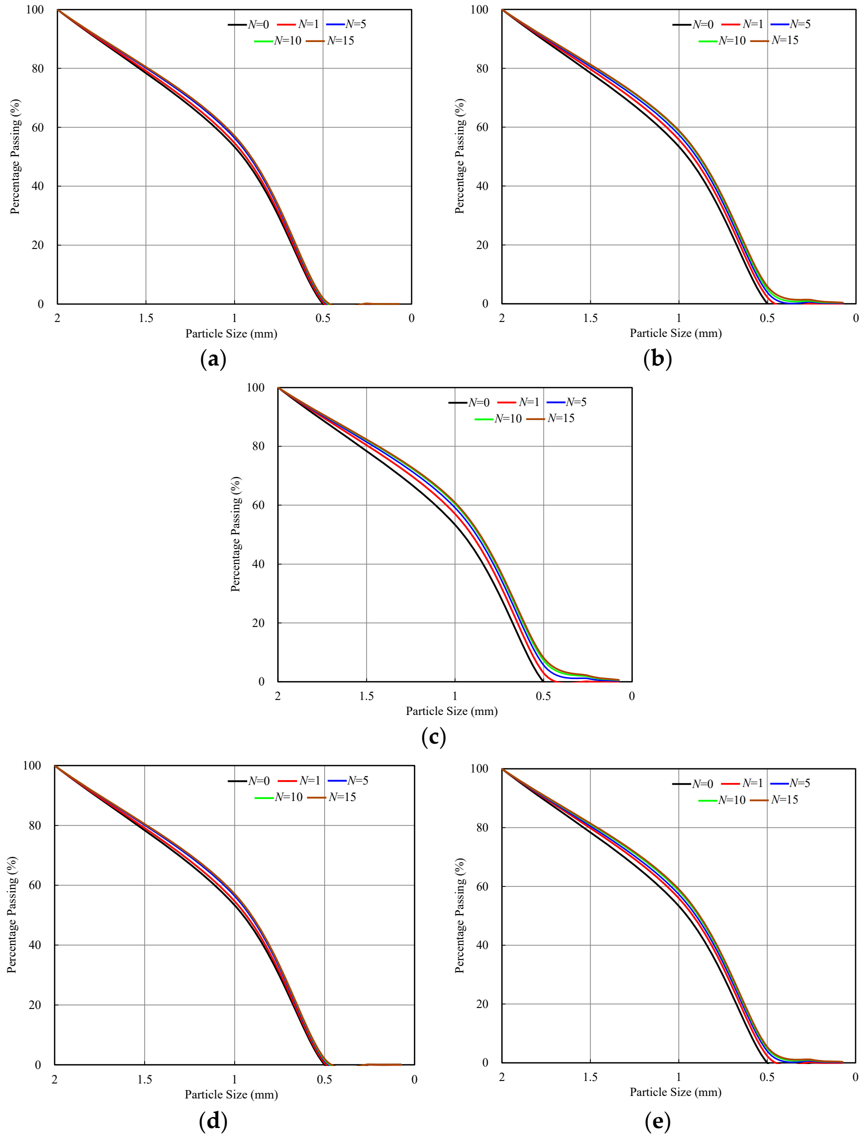

Figure 12. Particle grading curves under different cycles: (**a**) constant stress normal stress 200 kPa; (**b**) constant stress normal stress 1100 kPa; (**c**) constant stress normal stress 2400 kPa; (**d**) constant stiffness normal stress 200 kPa; (**e**) constant stiffness normal stress 1100 kPa.

4.2. Particle Breakage Evaluation

Particle breakage can cause changes in the gradation of granular soil. Hardin's breakage model was used to study the degree of particle breakage. This model refers to the initial breakage potential B_{po} as the area enclosed by the pretest gradation curve and the vertical line with a particle size of d = 0.5–2 mm. The total breakage B_{t} is the area enclosed by the post-test gradation curve and the vertical line with a particle size of d = 0.074 mm. The formula for the relative breakage value B_{r} is as follows:

$$B_{\mathrm{r}} = \frac{B_{\mathrm{t}}}{B_{\mathrm{po}}} \tag{2}$$

According to Formula (2), the relative breakage value of the test sand under different test conditions is calculated. The relationship between the relative breakage value and the number of cycles is shown in Figure 13. It can be seen that under the same number of cycles, the normal stress shows a positive correlation with the relative breakage value. Under the same normal stress, the relative breakage value B_{r} increases with the number of cycles, but the rate of increase gradually slows down, which indicates that the first few cycles caused significant particle breakage. As the number of cycles increases, the amount of breakage caused by shear behavior gradually decreases. The relative breakage values at 200 kPa, 1100 kPa, and 2400 kPa are concentrated in the range of 0.012~0.046, 0.029~0.074, and 0.046~0.101, respectively. The relative breakage values B_{r} under constant stress and constant stiffness conditions are relatively close.

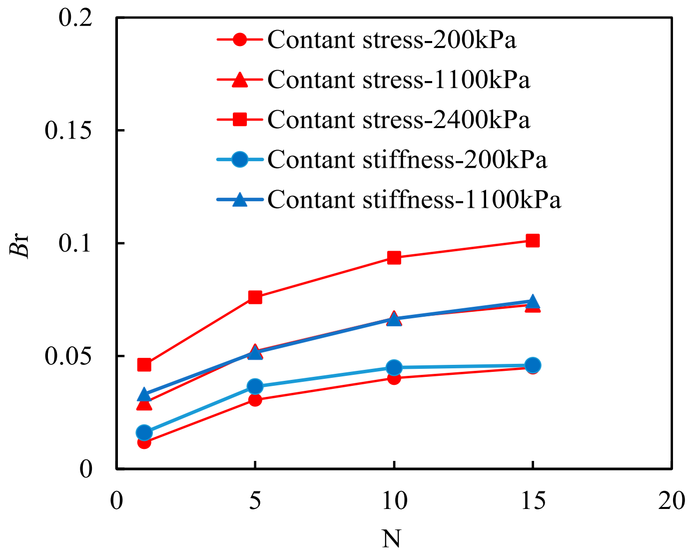

Figure 13. Relationship between relative breakage value and number of cycles.

4.3. Microscopic Characteristics of Crushed Particles

Conduct SEM electron microscopy tests on sand particles with particle sizes ranging from 0.25 to 0.5 mm, 0.075 to 0.25 mm, and <0.075 mm after screening, with magnification of 30 times, 100 times, and 500 times, as shown in Figure 14. For crushed siliceous sand particles, when magnified by 30 times for sand particles with a particle size range of 0.25~0.5 mm, multiple particles with obvious fractures and irregular shapes can be seen; no open pores are observed on the surface of the particles. In a photo magnified by 100 times, several particles with rough surfaces and fractures can be observed. In a photo magnified by 500 times, only smoother particle surfaces can be seen. When magnified 30 times for siliceous sand with a particle size range of 0.075~0.25 mm, many particles of varying sizes can be seen. The fracture surface of the particles can be clearly seen in a photo magnified by 100 times, and the fracture morphology of individual particles can be observed in a photo magnified by 500 times. Magnify siliceous sand smaller than 0.075 mm by 30 times, and countless small particles can be seen in the photo. The shape and size of the particles can only be clearly seen in the photo magnified by 100 times, and the particle size varies. There are multiple flaky siliceous sand particles in the photo magnified by 500 times.

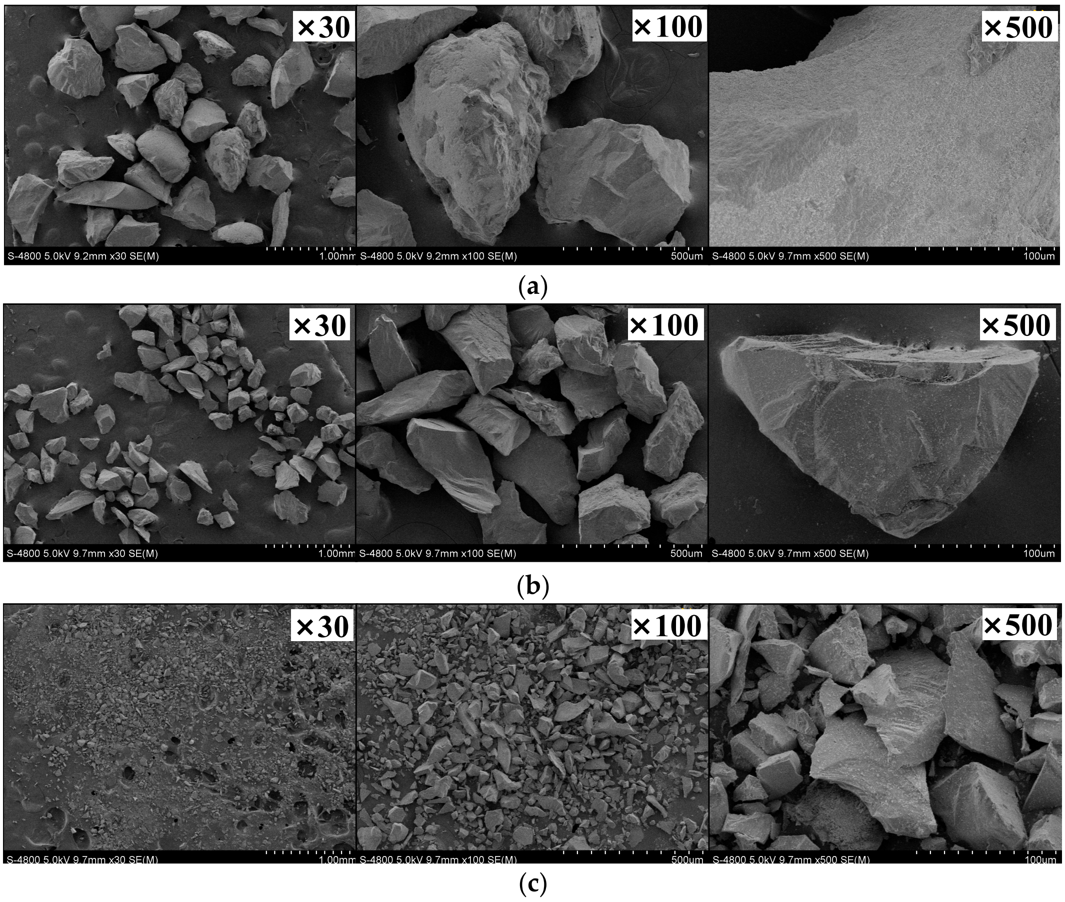

Figure 14. SEM images of crushed siliceous sand particles: (**a**) particle size range (0.25~0.5 mm); (**b**) particle size range (0.075~0.25 mm); (**c**) particle size range (<0.075 mm).

5. Numerical Simulation

Sand is a soil mass with anisotropy, nonuniformity, and discreteness. The mechanics and deformation characteristics of the structure–sand interface are closely related to the formation and evolution of shear bands. The discrete element method (DEM) is widely used in geotechnical engineering as a numerical analysis method to describe the mechanic characteristics of granular soil [31–33]. In this paper, the numerical analysis software PFC^{2D} 5.0 is used to simulate the cyclic shear test of the steel–sand interface, and the evolution law of the principal stress field and composition diagram is studied.

5.1. Model Assumptions

The assumptions of the numerical model include that all particles are rigid bodies, the particle shape is circular, contact particles can rotate with each other, the connection between particles is achieved through the use of tangent points, the contact state of particles is represented by the bonding force between particles, and a small overlap between particles is allowed.

5.2. Modeling

5.2.1. Setting of Generalized Walls

As shown in Figure 15, the upper shear box and structure are simulated through a generalized wall, which is consistent with the experimental size. The generalized wall size is set to be 100 mm long and 50 mm high. The numbers ①, ③, and ④ in the figure represent the upper shear box, while the number ② represents the structure. Taking a steel plate with 20 textures as an example, the texture size remains consistent with the test. During the experiment, the generalized wall numbered ①, ③, and ④ remained stationary, while the generalized wall numbered ② underwent bidirectional cyclic shear at a certain shear rate.

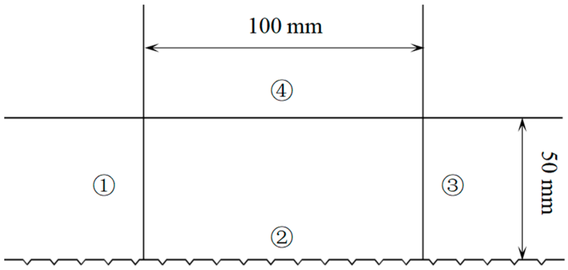

Figure 15. Setting of generalized walls.

5.2.2. Generate Particles

The establishment of the numerical simulation experimental model adopts the GM method proposed by Duan and Cheng [34]. According to this method, the grid is divided layer by layer from the interface and filled with particles.

5.2.3. Determination of Numerical Simulation Parameters

Considering that particles may undergo fragmentation under different experimental conditions, the study of model fragmentation is achieved through the method of breaking the bond chain between particles. Therefore, the initial grading of the model needs to be input according to the grading after experimental fragmentation. Hardin [35] found that particles with a particle size of less than 0.074 mm no longer break. Therefore, the minimum particle size after crushing was set to 0.074 mm, and the initial model grading curve is shown in Figure 16.

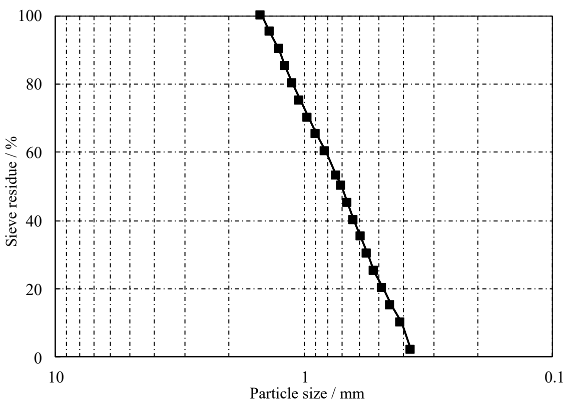

Figure 16. The initial grading curve of the model.

The contact between particles or between particles and structure adopts a linear stiffness model. The linear stiffness model is expressed as the relationship between the contact force and the relative displacement of particles, which includes the relationship between the normal contact force and the normal displacement, and the relationship between the tangential contact force and the tangential displacement. The formula is as follows:

$$\left.\begin{aligned} F_i^n &= k_n U^n n_i \\ \Delta F_i^s &= -k_s \Delta U_i^s \end{aligned}\right\} \tag{3}$$

In the above formula, k_n and k_s are the normal contact stiffness and tangential contact stiffness, respectively; n_i is the normal vector; U^n and U^s are the increment of normal contact force and tangential contact force; and are the increment of normal displacement and tangential displacement.

The friction coefficient μ between particles or between structures and particles through indoor experiments is shown in Table 4, and the numerical simulation parameters are shown in Table 5.

Table 4. Friction coefficient μ.

Contact Type	Loading Method	Friction Coefficient μ
between particles	constant stress constant stiffness	0.6551 0.7209
between particles and structure	constant stress constant stiffness	0.5589 0.6223

Table 5. Numerical simulation parameters.

Particle Density ρ/(kg/m^3)	Tangential Contact Stiffness between Particles k_s/(N/m)	Normal Contact Stiffness between Particles k_n/(N/m)	Normal Contact Stiffness of Wall k_{nw}/(N/m)	Initial Porosity n_0
1628	1×10^8	1×10^8	4×10^8	0.23

5.2.4. Setting of the Bonding Model

The study of particle fragmentation characteristics is achieved by constructing a bonding model [36], as shown in Figure 17. A bonding chain is added between circular particles generated by the GM method, which sets point contact between particles and randomly binds multiple small particles into a square particle unit with a side length of 1 mm. The particle units are separated by a bonding interval value. The higher the normal stress, the smaller the bonding interval value, and the closer the contact between particles.

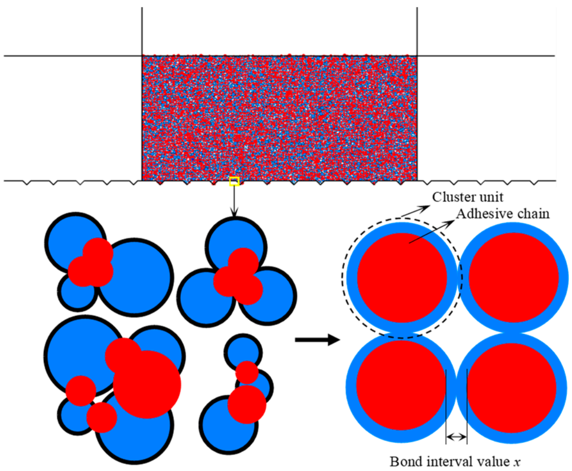

Figure 17. Setting of the bonding model.

As shown in Figure 18, during the preloading or shear process of the square particle unit, some of the bonding chains in the particle unit are broken, the red circles disappear, and smaller particle units are generated. As the agglomerates generated by this method are closer to the actual sand particles, the model calculation results are more reliable. By adjusting the model parameters, the bonding force between silica sand particles is set to 4200 N.

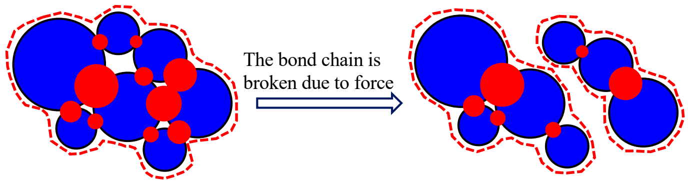

Figure 18. Schematic diagram of model particle broken.

5.2.5. Arrangement of Measuring Circles and Principal Stresses

As shown in Figure 19, using the measurement circle function in PFC^{2D}, a total of one hundred and twelve measurement circles with fourteen rows and eight columns were set inside the particles to monitor the stress changes of the particles under different cycles. UD Tensor was used inside each measurement circle to set the principal stress, with the long axis representing the large principal stress and the short axis representing the small principal stress. The magnitude of the principal stress is related to the trace of the stress tensor, and the larger its shape, the greater the particle stress value.

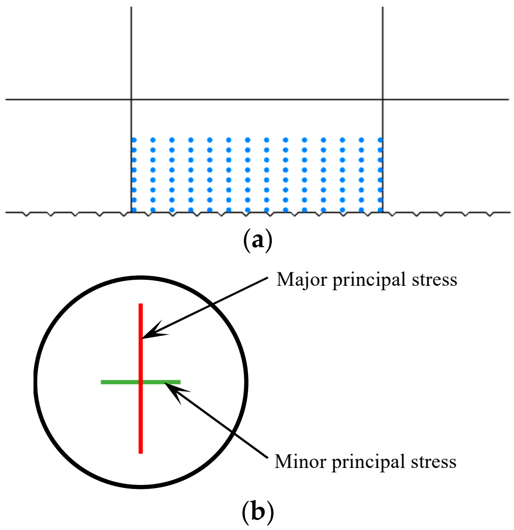

Figure 19. Arrangement of measuring circles and principal stresses: (**a**) arrangement of measuring circles; (**b**) arrangement of principal stresses.

5.3. Experimental Plan for Numerical Simulation

The experimental plan of numerical simulation is consistent with the indoor experiment, with a total of 20 sets of experiments.

5.4. Numerical Simulation Results

5.4.1. Model Reliability Verification

As shown in Figure 20, taking the relationship between shear stress at the interface of steel siliceous sand and the number of cycles at a constant stiffness of 200 kPa as an example, a comparison was made between indoor experimental data and numerical simulation data. It can be seen that the model shear stress shows a regular fluctuation with an increase in the number of cycles, and the peak shear stress of the model showing a trend of first decreasing and then gradually stabilizing with an increase in the number of cycles. This is basically consistent with the variation pattern of experimental data.

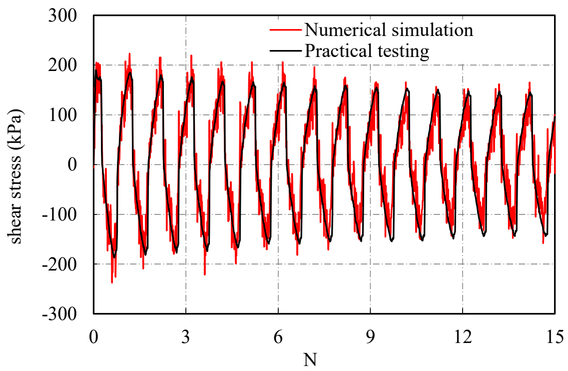

Figure 20. Verification of the relationship between interface shear stress and number of cycles.

5.4.2. Evolution of Principal Stress Field

The evolution of the principal stress field under different normal stresses is shown in Figure 21. The red long axis in the figure represents the large principal stress, and the green short axis represents the small principal stress. During the sand preloading pro-cess, the vertical direction is the large principal stress, and the horizontal direction is the small principal stress. It can be concluded that the size and rotation of the princi-pal stress show different laws with the increase of normal stress and the number of cy-cles. At 200 kPa, the length of the principal stress in most areas of the figure is small, which means that the contact force between sand particles is small. The occurrence of high principal stress and significant deflection is mainly concentrated in the middle region, and the magnitude and deflection of principal stress under the 10th and 15th cycle are more significant than those under the 1th and 5th cycle. At 1100 kPa and 2400 kPa, the principal stress is larger, which means that the contact force between particles is larger, but the deflection angle of the principal stress is smaller than that at 200 kPa, and the principal stress with large angle deflection is mainly concentrated near the interface, which means that the particles contact more closely under high normal stress than under low normal stress, and the principal stress is more difficult to produce rotation. The size of the principal stress and deflection angle under the first cycle are smaller than those under the 5th, 10th and 15th cycles.

5.4.3. Evolution of Composition Diagram

In the cyclic shear test, the contact force between particles and the direction of the principal stress change with the number of cycles. The number of particles in different directions is counted as an interval of 5°, and the statistical data is plotted in polar co-ordinates to form a composition diagram. The composition diagram reflects the arrangement characteristics of the contact between particles in space. Therefore, through the study of the composition diagram, the variation law of the sand particle contact number with angle, cycle times, and normal stress can be obtained, and the anisotropy degree of the contact force and contact number distribution can be analyzed accordingly.

The composition diagram of the interface is shown in Figure 22. It can be analyzed that under the same cycle number, the contact numbers at different angles are connected to form an asymmetric circle line composed of multiple straight lines, and the sand particles show obvious anisotropic characteristics. The composition diagram does not show an obvious change law with the number of cycles. The number of particles in each direction is increasing with the normal stress, which is reflected in the increase in the composition area. This indicates that the contact force between particles is positively correlated with the normal stress. Under the same normal stress, there is little difference in the number of contacts in different directions under constant stress and constant stiffness loading conditions.

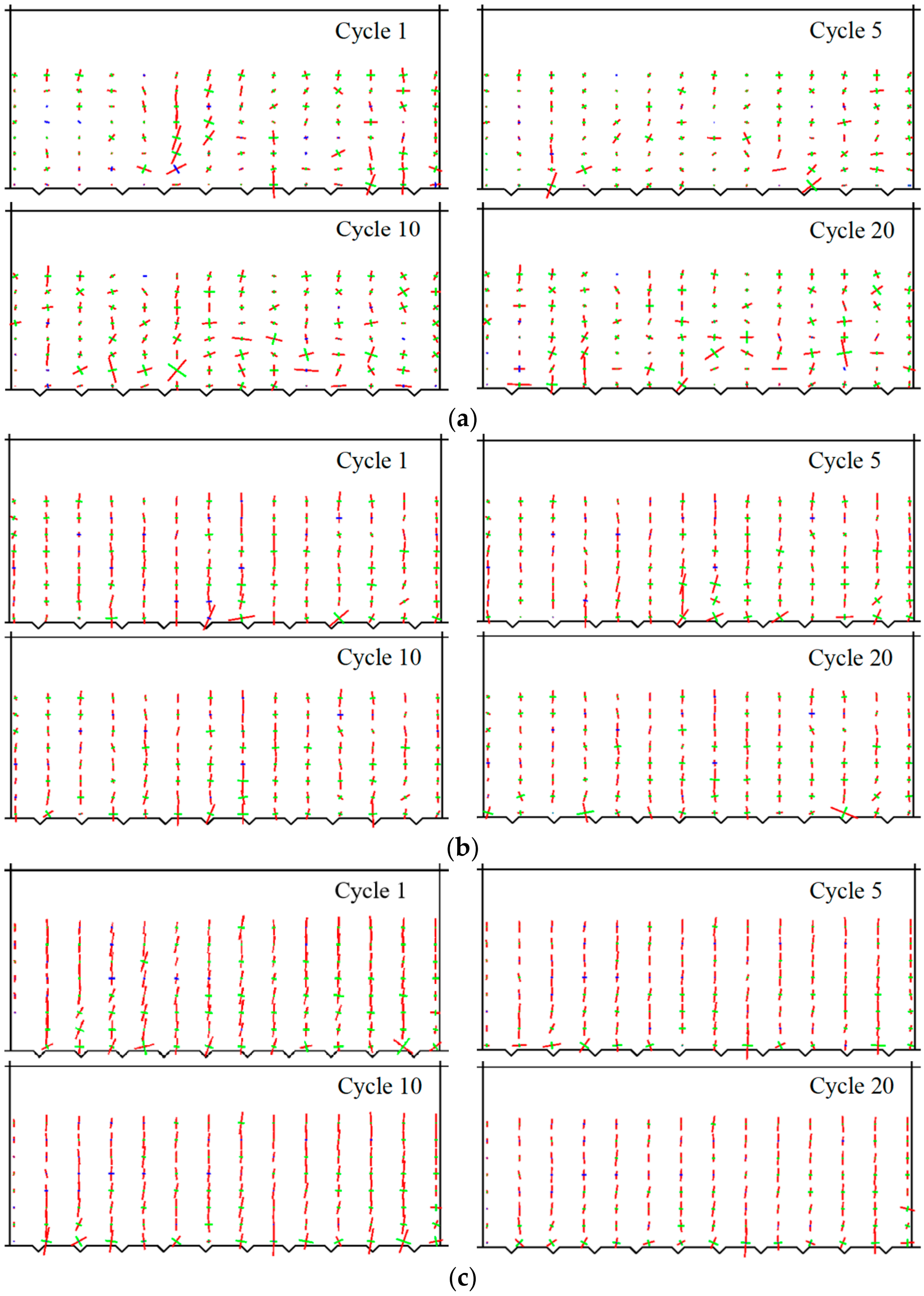

Figure 21. Evolution of interface principal stress field under constant stress: (**a**) 200 kPa; (**b**) 1100 kPa; (**c**) 2400 kPa.

Taking 90° as a statistical interval, calculate the average contact number within the range of 0° to 90°, 90° to 180°, 180° to 270°, and 270° to 360°. The relationship between the average contact number and the number of cycles is shown in Figure 23. It can be concluded that the average contact number is the highest in the range of 270° to 360°, the lowest in the range of 90° to 180°, and the average contact number is relatively close between the range of 0° to 90° and the range of 180° to 270°. The average contact number between particles fluctuates within a certain range as the number of cycles increases at 200 kPa. At 1100 kPa and 2400 kPa, there is a small change from the beginning of the experiment to the end of the first cycle. The average contact number from the first cycle to the fifteenth cycle remains at a stable value. The above law is the same as the law of the principal stress field under different normal stresses.

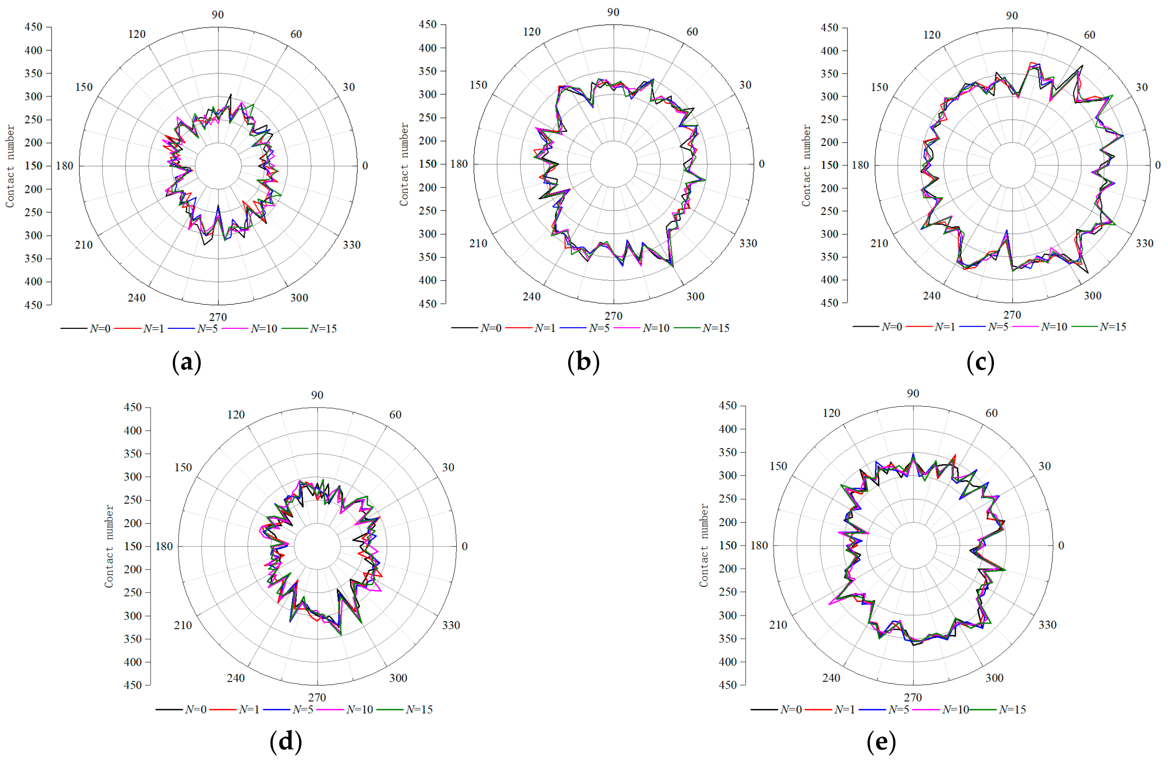

Figure 22. Composition diagram of interface: (**a**) constant stress 200 kPa; (**b**) constant stress 1100 kPa; (**c**) constant stress 2400 kPa; (**d**) constant stiffness 200 kPa; (**e**) constant stiffness 1100 kPa.

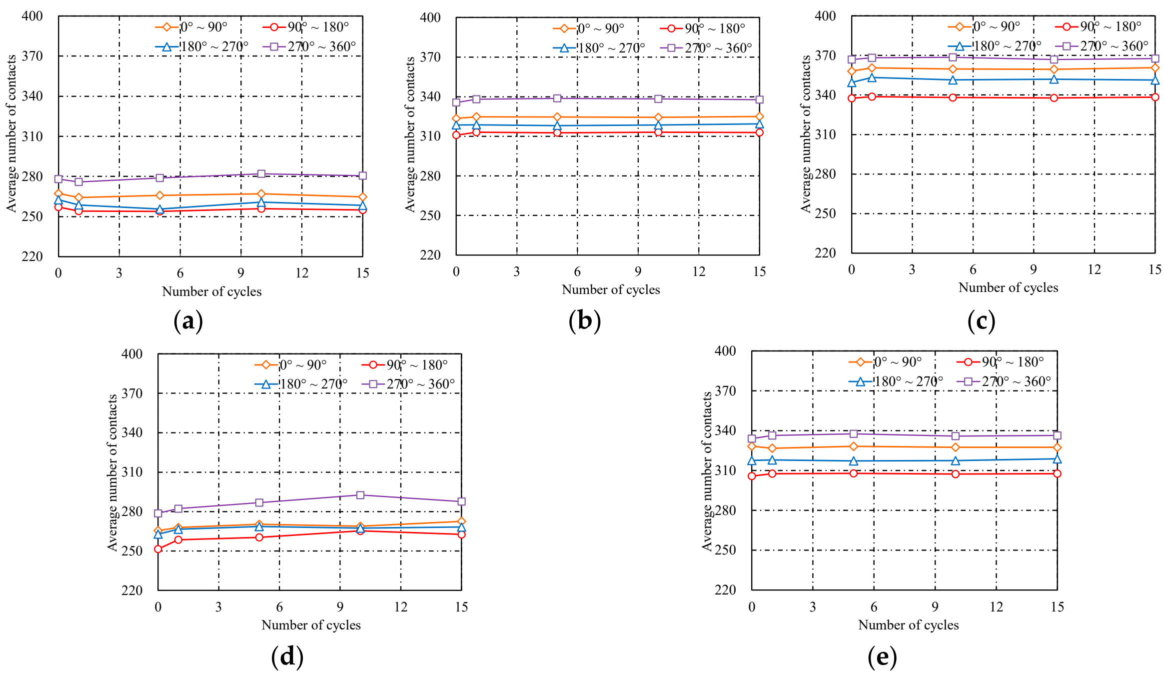

Figure 23. The relationship between the average contact number and the number of cycles: (**a**) constant stress 200 kPa; (**b**) constant stress 1100 kPa; (**c**) constant stress 2400 kPa; (**d**) constant stiffness 200 kPa; (**e**) constant stiffness 1100 kPa.

6. Conclusions

Cyclic shear tests were conducted between steel and siliceous sand using self-developed large-scale direct shear equipment, and the macroscopic shear characteristics of the interface and particle breakage characteristics were studied. Finally, numerical simulation software was used to analyze the interface shear characteristics under cyclic loading. The following conclusions were obtained:

(1) Under constant stress conditions, the peak shear stress at low and medium pressure first increases and then decreases with the number of cycles. The peak shear stress at high pressure increases with the number of cycles. Under constant stiffness conditions, the peak shear stress at medium and low pressure decreases with the increase of the number of cycles. The variation rule of the area of the "hysteresis loop" formed by the relationship curve between shear stress and shear displacement is the same as the interface peak shear stress.
(2) The volumetric characteristics of siliceous sand exhibit shear shrinkage in each cycle as a whole. As the number of cycles increases, the shear shrinkage volume variable gradually decreases, and the cumulative shear shrinkage volume variable increases with normal stress. The amplitude of the fluctuation of the relationship curve between normal displacement and shear displacement decreases with the number of cycles, and the shape of the curve varies under low, medium, and high pressure.
(3) As the number of cycles increases, the relationship curve between shear stress and normal stress gradually moves towards the direction of low normal stress, and the distance between the curves of different cycles gradually decreases with the number of cycles.
(4) Under constant stress conditions, the variation rule of the interface friction angle with the number of cycles and normal stress is the same as that of peak shear stress. However, under constant stiffness conditions, the interface friction angle at low pressure increases with the number of cycles, while the interface friction angle at medium pressure first decreases and then stabilizes with the number of cycles.
(5) The relative breakage value increases with the number of cycles, but the rate of increase gradually slows down, and the breakage amount of a single cycle caused by shear behavior gradually decreases. The broken particles have obvious cracks and irregular shapes, and no open pores are observed on the surface of the particles. A large number of flaky particles appear in the sand with a particle size of less than 0.075 mm.
(6) The principal stress increases with the normal stress, but its rotation degree gradually reduces with the normal stress. The principal stress of large angle deflection is mainly concentrated near the interface at 1100 kPa and 2400 kPa, which is related to an increase in the normal stress, the close contact between particles, and an increase in the contact force.
(7) The contact number of particles at different angles increases with the normal stress. Sand particles exhibit obvious anisotropic characteristics under different experimental conditions. The average contact number between 270° and 360° is the highest, while the average contact number between 90° and 180° is the lowest; the remaining two intervals are relatively close.

Author Contributions: Conceptualization, Y.M. and J.G.; methodology, Y.M. and J.G.; investigation, Y.M. and R.W.; resources, J.G. and R.W.; data curation, Y.M.; writing—original draft preparation, J.G. and R.W.; writing—review and editing, Q.Z. (Qingyao Zhang) and Q.Z. (Qingxin Zhang); visualization, R.W. and S.Z.; supervision, J.G. and J.L.; funding acquisition, J.L. and S.Z. All authors have read and agreed to the published version of the manuscript.

Funding: This research was funded by the Shandong Natural Science Foundation (ZR2020QE257), the Transportation technology project of Shandong Province (no. 2020B23), and Shandong Jiaotong University Graduate Science and Technology Innovation Project (2022YK022).

Data Availability Statement: Data will be made available on request.

Acknowledgments: The support of the Natural Foundation of Shandong Province and the Shandong Jiaotong University is highly appreciated.

Conflicts of Interest: The authors declare no conflict of interest.

References

1. Xiao, Y.; Wang, C.; Zhang, Z.; Liu, H.; Yin, Z. Constitutive modeling for two sands under high pressure. *Int. J. Geomech.* **2021**, *21*, 04021042. [CrossRef]
2. Zhu, J.-F.; Zhao, H.-Y.; Xu, R.-Q.; Luo, Z.-Y.; Jeng, D.-S. Constitutive modeling of physical properties of coastal sand during tunneling construction disturbance. *J. Mar. Sci. Eng.* **2021**, *9*, 167. [CrossRef]
3. Güner, F.; Başer, V.; Zenk, H. Evaluation of offshore wind power plant sustainability: A case study of sinop/gerze, Turkey. *Int. J. Glob. Warm.* **2021**, *23*, 370. [CrossRef]
4. Thorsten, H.; Kuenzer, C. Global dynamics of the offshore wind energy sector monitored with sentinel-1: Turbine count, installed capacity and site specifications. *Int. J. Appl. Earth Obs. Geoinf.* **2022**, *112*, 102957. [CrossRef]
5. Li, L.; Liu, H.; Wu, W.; Wen, M.; El Naggar, M.H.; Yang, Y. Investigation on the behavior of hybrid pile foundation and its surrounding soil during cyclic lateral loading. *Ocean. Eng.* **2021**, *240*, 110006. [CrossRef]
6. Zhang, X.L.; Liu, C.R.; Wang, P.G.; Zhang, G.L. Experimental simulation study on dynamic response of offshore wind power pile foundation under complex marine loadings. *Soil Dyn. Earthq. Eng.* **2022**, *156*, 107232. [CrossRef]
7. Zhang, J.; Wang, H. Development of offshore wind power and foundation technology for offshore wind turbines in China. *Ocean. Eng.* **2022**, *266*, 113256. [CrossRef]
8. Ding, X.; Deng, X.; Ou, Q.; Deng, W. Experimental study on the behavior of single pile foundation under vertical cyclic load in coral sand. *Ocean. Eng.* **2023**, *280*, 114672. [CrossRef]
9. Chin, J.T.; Poulos, H.G. Tests on Model Jacked Piles in Calcareous Sand. *Geotech. Test. J.* **1996**, *19*, 1520. Available online: https://www.astm.org/gtj10339j.html (accessed on 4 May 2023).
10. Zhu, W.; Ye, G.; Gu, L.; Zhang, F. 1g model test of piled-raft foundation subjected to vibration load and its simulation considering small confining stress. *Soil Dyn. Earthq. Eng.* **2022**, *156*, 107212. [CrossRef]
11. Zhao, X.; Xue, J.; Han, Y.; Chen, S. Model test study on horizontal bearing behavior of pile under existing vertical load. *Soil Dyn. Earthq. Eng.* **2021**, *147*, 106820.
12. Ding, Z.; Song, C.; Chen, L.; Shi, K. Dynamic analysis of laterally loaded single piles in sandy soils considering sliding and debonding on the pile-soil interface. *Ocean. Eng.* **2020**, *217*, 107720. [CrossRef]
13. Bekki, H.; Canou, J.; Tali, B.; Dupla, J.-C.; Bouafia, A. Evolution of local friction along a model pile shaft in a calibration chamber for a large number of loading cycles. *Comptes Rendus Mec.* **2013**, *341*, 499–507. [CrossRef]
14. Bekki, H.; Canou, J.; Tali, B.; Dupla, J.C.; Bouafia, A. Parametric study of the evolution of shaft friction of a model pile in calibration chamber subjected to cyclic loading at a large number of cycles. *Eur. J. Environ. Civ. Eng.* **2020**, *26*, 2400–2416. [CrossRef]
15. Zheng, Z.; El Naggar, M.H.; Wang, J.L.; Yang, Q. Coupling effect of roughness and normal pressure on mechanical characteristics and failure mode of deep-sea sediment interface. *Ocean. Eng.* **2023**, *267*, 113255. [CrossRef]
16. Silva, C.L.; Koseki, J.; Wahyudi, S.; Sato, T. Stress–dilatancy relationships of sand in the simulation of volumetric behavior during cyclic torsional shear loadings. *Soils Found.* **2014**, *54*, 845–858. [CrossRef]
17. Tarhouni, M.; Hawlader, B. Monotonic and cyclic behaviour of sand in direct simple shear test conditions considering low stresses. *Soil Dyn. Earthq. Eng.* **2021**, *150*, 106931. [CrossRef]
18. Zhao, L.; Yang, P.; Zhang, L.-C.; Wang, J. Cyclic direct shear behaviors of an artificial frozen soil-structure interface under constant normal stress and sub-zero temperature. *Cold Reg. Sci. Technol.* **2017**, *133*, 70–81. [CrossRef]
19. Maghool, F.; Arulrajah, A.; Mirzababaei, M.; Suksiripattanapong, C.; Horpibulsuk, S. Interface shear strength properties of geogrid-reinforced steel slags using a large-scale direct shear testing apparatus. *Geotext. Geomembr.* **2020**, *48*, 625–633. [CrossRef]
20. Xiao, S.; Suleiman, M.T.; Al-Khawaja, M. Investigation of effects of temperature cycles on soil-concrete interface behavior using direct shear tests. *Soils Found.* **2019**, *59*, 1213–1227. [CrossRef]
21. Wang, J.; Liu, F.; Wang, P.; Cai, Y. Particle size effects on coarse soil-geogrid interface response in cyclic and post-cyclic direct shear tests. *Geotext. Geomembr.* **2016**, *44*, 854–861. [CrossRef]
22. White, D.J.; Bolton, M.D. Displacement and strain paths during plane-strain model pile installation in sand. *Géotechnique* **2004**, *54*, 375–397. [CrossRef]
23. Yu, F.; Yang, J. Improved Evaluation of Interface Friction on Steel Pipe Pile in Sand. *J. Perform. Constr. Facil.* **2012**, *26*, 170–179. [CrossRef]
24. Liu, J.; Cui, L.; Zhu, N.; Han, B. Investigation of cyclic pile-sand interface weakening mechanism based on large-scale cns cyclic direct shear tests. *Ocean. Eng.* **2019**, *194*, 106650. [CrossRef]
25. Vangla, P.; Gali, M.L. Effect of particle size of sand and surface asperities of reinforcement on their interface shear behavior. *Geotext. Geomembr.* **2016**, *44*, 254–268. [CrossRef]
26. Vangla, P.; Gali, M.L. Effects of interface roughness, particle geometry and gradation on the sand–steel interface friction angle. *J. Geotech. Geoenviron. Eng.* **2018**, *144*, 04018096. [CrossRef]
27. Rui, S.; Wang, L.; Guo, Z.; Zhou, W.; Li, Y. Cyclic behavior of interface shear between carbonate sand and steel. *Acta Geotech. Int. J. Geoengin.* **2021**, *16*, 189–209. [CrossRef]
28. Tohidvand, H.R.; Hajialilue-Bonab, M.; Katebi, H.; Nikvand, V.; Ebrahimi-Asl, M. Monotonic and post cyclic behavior of sands under different strain paths in direct simple shear tests. *Eng. Geol.* **2022**, *302*, 106639. [CrossRef]

29. Al Tarhouni, M.A.; Hawlader, B. Drained cyclic behaviour and state-dependent stress–dilatancy relationship of sand in direct simple shear tests. *Soil Dyn. Earthq. Eng.* **2023**, *168*, 107801. [CrossRef]
30. *JTG 3430-202.2020-08-10*; Test Methods of Soils for Highway Engineering. Institute of Highway Research, Ministry of Transport: Beijing, China, 2020.
31. Jiang, M.J.; Yu, H.S.; Harris, D. Bond rolling resistance and its effect on yielding of bonded granulates by DEM analyses. *Int. J. Numer. Anal. Methods Geomech.* **2006**, *30*, 723–761. [CrossRef]
32. Wang, J.; Dove, J.E.; Gutierrez, M.S. Discrete-continuum analysis of shear banding in the direct shear test. *Géotechnique* **2007**, *57*, 513–526. [CrossRef]
33. Zhou, W.-H.; Jing, X.-Y.; Yin, Z.-Y.; Geng, X. Effects of particle sphericity and initial fabric on the shearing behavior of soil-rough structural interface. *Acta Geotechnol.* **2019**, *14*, 1699–1716. [CrossRef]
34. Duan, N.; Yi, P.C. A modified method of generating specimens for a 2D DEM centrifuge model. In *Geo-Chicago*; American Society of Civil Engineers: Reston, VA, USA, 2016; pp. 610–620. [CrossRef]
35. Hardin, B.O. Crushing of soil particles. *J. Geotech. Eng.* **1985**, *111*, 1177–1192. [CrossRef]
36. Potyondy, D.O.; Cundall, P.A. A bonded-particle model for rock. *Int. J. Rock Mech. Min. Sci.* **2004**, *41*, 1329–1364. [CrossRef]